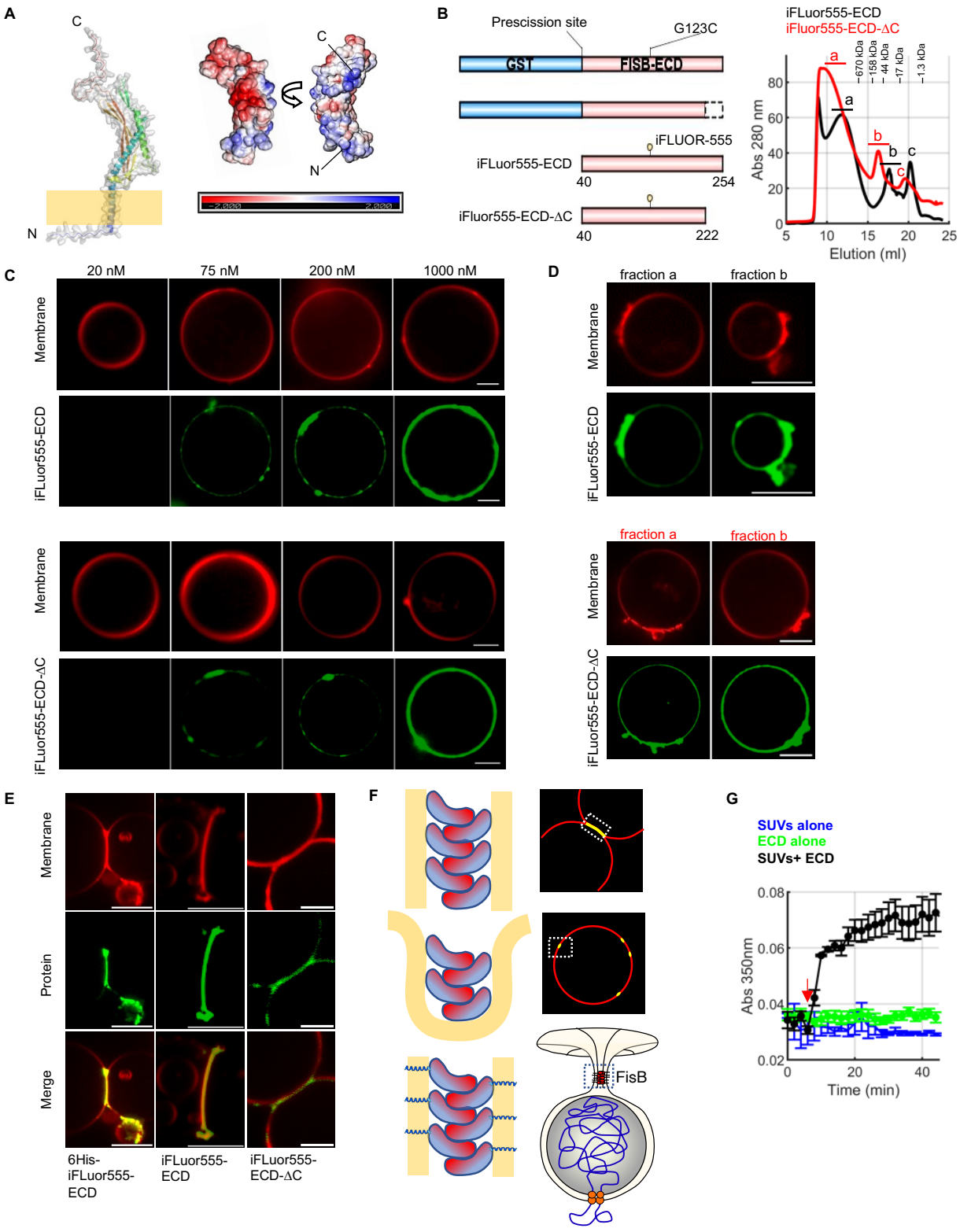

Figure S1. Self-aggregation, lipid binding, and membrane bridging of FisB ECD occur in the absence of a purification tag and the carboxy-terminal region. Related to Figure 2. A. Left: AlphaFold[S1,S2] model of FisB (https://alphafold.com/entry/O32131). The membrane is shown schematically. Right: electrostatic potential of FisB ECD (residues 44-225, computed

using PyMOL (Delano Scientific LLC) plugin APBS). **B**. Left. Domain structure of the GST-FisB ECD fusion proteins generated. A Prescission protease site allows on-column cleavage of the GST tag and purification of a tag-free protein. A construct lacking the last 31 residues (FisB-ECD ΔC), predicted to be disordered (see A), was also generated. In both cases, a point mutation (G123C) allowed site-specific fluorescent labelling with iFluor555 maleimide (FisB-ECD does not have any endogenous cysteines). Right: gel filtration elution profiles in Superose 6 Increase 10/300 GL column indicate formation of soluble aggregates as for His_6-tagged FisB ECD[3], suggesting self-aggregation is not due to the disordered C-terminus or the GST-tag. Elution volumes of molecular weight markers are indicated. **C**. Binding of FisB-ECD or FisB-ECD ΔC to giant unilamellar vesicle (GUV) membranes composed of (all mole %) *E.coli* PE : *E.coli* CL : *E.coli* PG : EggPC : Cy5-PC = 25:5:50:19:1). Proteins eluted from glutathione Sepharose 4B beads upon protease cleavage were concentrated, labelled with iFluor555 maleimide and added to the GUV suspension at the indicated final concentrations. At low concentrations, FisB ECD forms small mobile clusters on membranes. With increasing concentration, labeling becomes more uniform and intense, indicating higher coverage of the membrane by the labeled protein. No membrane remodeling is visible even at high coverage, but increased lipid signals are frequently found where protein signals are also elevated. **D.** Different soluble aggregates bind similarly to GUV membranes. Protein eluted from beads was subjected to gel filtration and fractions were collected as shown in B and added to GUVs (final concentration ~500 nM). The third peak (c) in B contains low molecular weight degradation products and contaminants and was excluded from further analysis. **E.** All FisB ECD constructs tested caused adhesion between GUV membranes, with protein signals enhanced at adhesion patches. **F.** Hypothetical model of FisB ECD aggregation and membrane binding and how the geometry of FisB ECD oligomers on a GUV may relate to the geometry of full-length FisB aggregates within the bacterial membrane neck that undergoes fission. Schematics show how similar FisB ECD interactions with membranes and other FisB ECD molecules may underlie the observed membrane bridging (top) and aggregation on GUV membranes (middle), or the bacterial neck that is destined for scission (bottom). For each case, a speculative arrangement of FisB clusters and membranes is shown on the left for the region indicated by a dashed box on the right. Other modes of binding and aggegation states are also possible, which may explain the more uniform labeling observed at high GUV membrane coverage. **G**. Membrane bridging activity of tag-free FisB-ECD is similar to that of its His_6-tagged counterpart[3]. Small unilamellar vesicles (SUVs, in mole %: 25 *E. coli* PE, 5 *E. coli* CL, 50 *E. coli* PG, 19 eggPC, 50 μM total lipid) were incubated in the absence or presence of unlabeled FisB ECD. SUV aggregation was monitored by absorbance at 350 nm which increases due to increased scattering upon SUV aggregation. FisB was added at 5 minutes (1 μM final), which caused the absorbance to increase, indicating increased liposome aggregation. Scale bar: 5 μm.

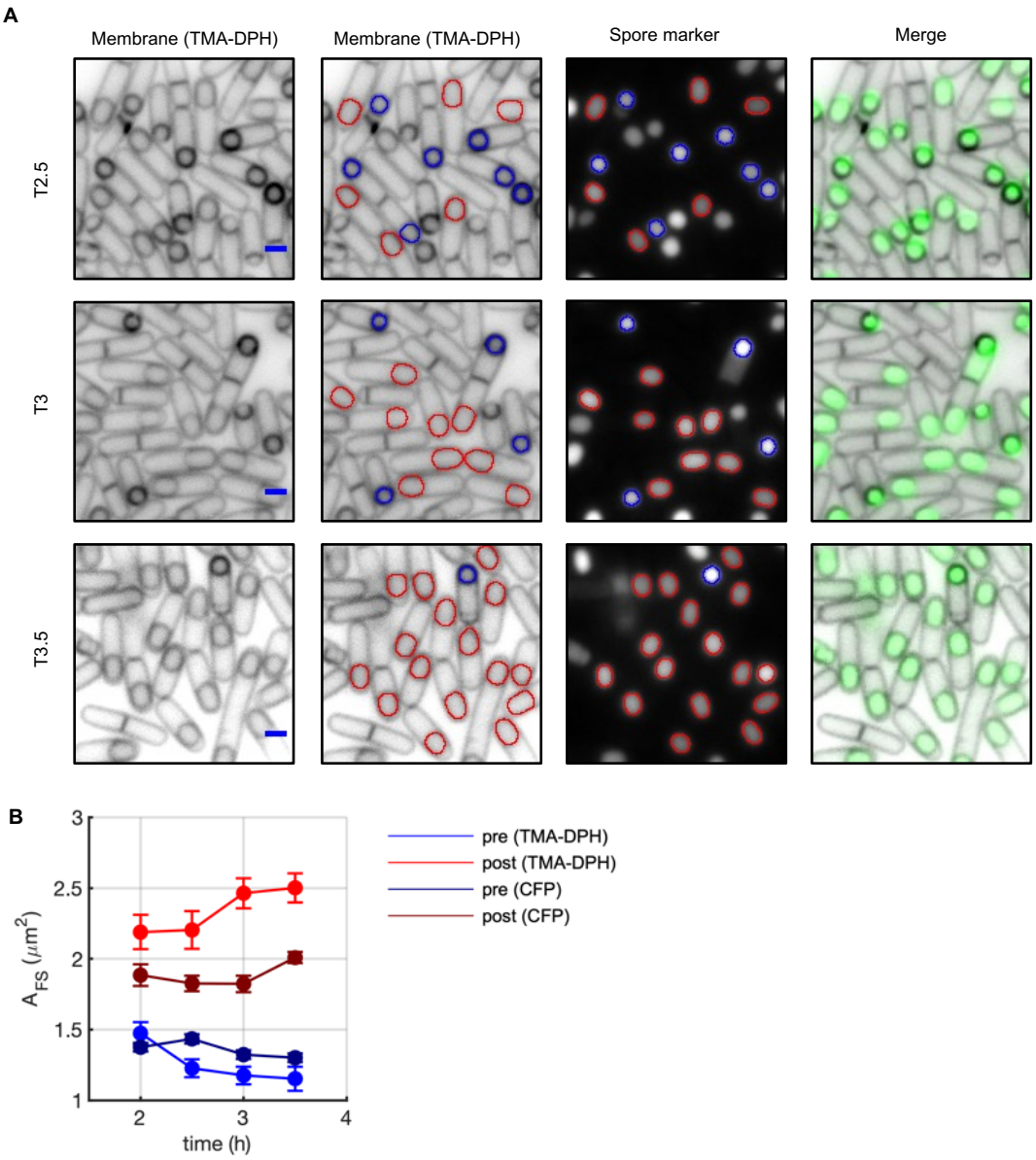

Figure S2. Forespore area changes can also be detected using a soluble marker. Related to Figure 3. A. Membrane fission was assessed by fluorescent microscopy during a sporulation time course in wild type (BKM015) cells containing a fluorescent forespore reporter (P_{spoIIQ}-*cfp*). Membranes were visualized with the fluorescent dye TMA-DPH. Forespore contours in pre- and post-fission cells are indicated with blue or red contours, respectively. Time (in hours) after the initiation of sporulation is indicated as T2.5, T3, etc.. Bar, 1 μm. **B.** Average post-fission forespore areas (A_{FS}) detected using either marker grow while average pre-fission FS areas shrink as a function of time into sporulation. Error bars represent SEM from three independent experiments (70 cells were analyzed per point).

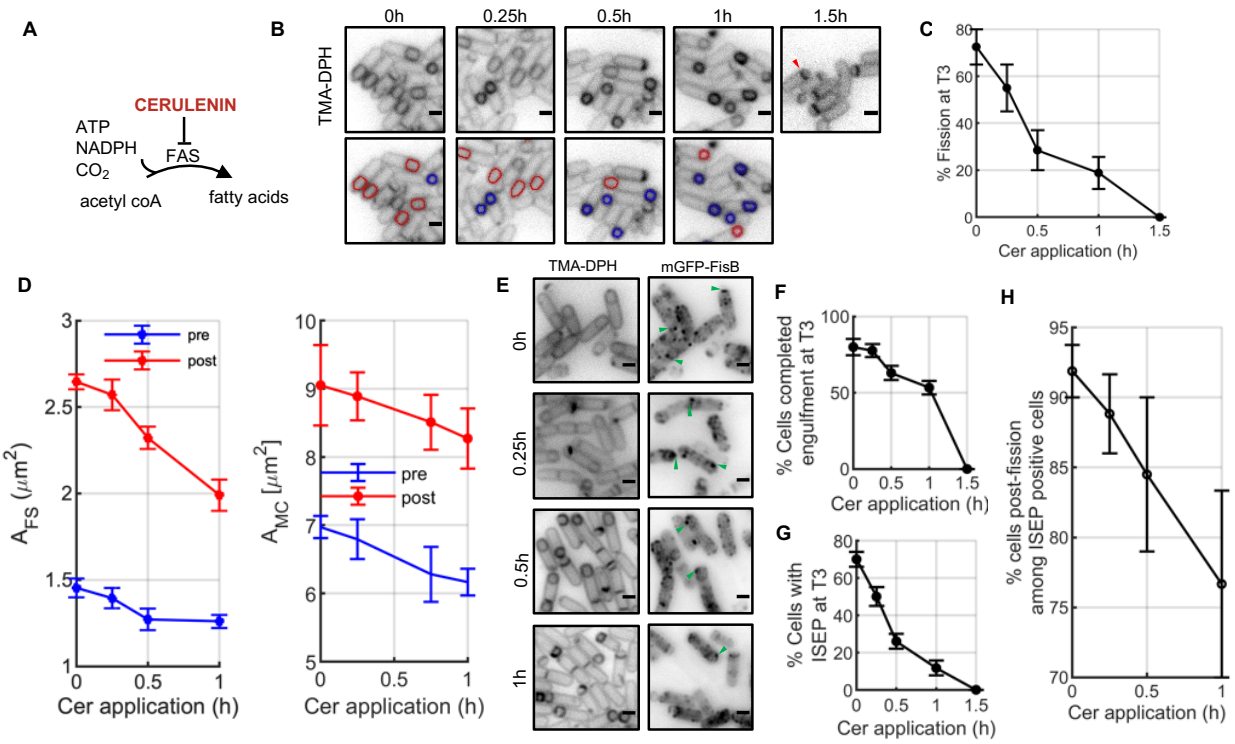

Figure S3. Blocking lipid synthesis inhibits forespore inflation and membrane fission. Related to Figure 4. A. Cerulenin (Cer) inhibits *de novo* synthesis of neutral lipids and phospholipids by inhibiting *de novo* fatty acid biosynthesis. **B.** Representative images showing cells at *t* = 3 h after addition of 10 µg/ml cerulenin at indicated timepoints after nutrient downshift. Membranes were visualized with TMA-DPH. A cell that is blocked at the asymmetric division stage is highlighted (red arrowhead). Scale bars = 1 µm**. C.** Percentage of cells (wild-type strain, PY79) that have undergone membrane fission at *t* = 3 h after addition of cerulenin at the indicated timepoints. More than 300 cells were analyzed for each time point. **D**. Quantification of forespore and mother cell membrane area for cells that have (red) or have not (blue) undergone membrane fission at *t* = 3 h after cerulenin addition at the indicated times after nutrient downshift (n=25-70 cells per data point). **E.** Fractional area occupied by the FS in pre- (blue) and post-fission (red) cells at t = 3 h. Cerulenin was added at the indicated times after nutrient downshift (n=25-70 cells per data point). **F**. Representative images showing cells (strain BAM003) at t=3 hr after the nutrient downshift, with Cer application for the indicated durations. Examples of cells with a discrete mGFP-FisB focus at the cell pole are highlighted with green arrowheads. Scale bars represent 1 µm. **G.** Engulfment is perturbed to a greater extent when lipid synthesis is inhibited earlier by cerulenin addition (>300 cells per data point). **H**. Percentage of cells with FisB accumulation (ISEP formation) at the membrane fission site, for cells that have visually completed engulment. **I**. The fraction of post-fission cells among cells with correct FisB localization (ISEP formation) as a function of increasing cerulenin application time (n=90-200 cells were analyzed per point). Means±SEM of 3 independent experiments are shown for panels C-E and G-I.

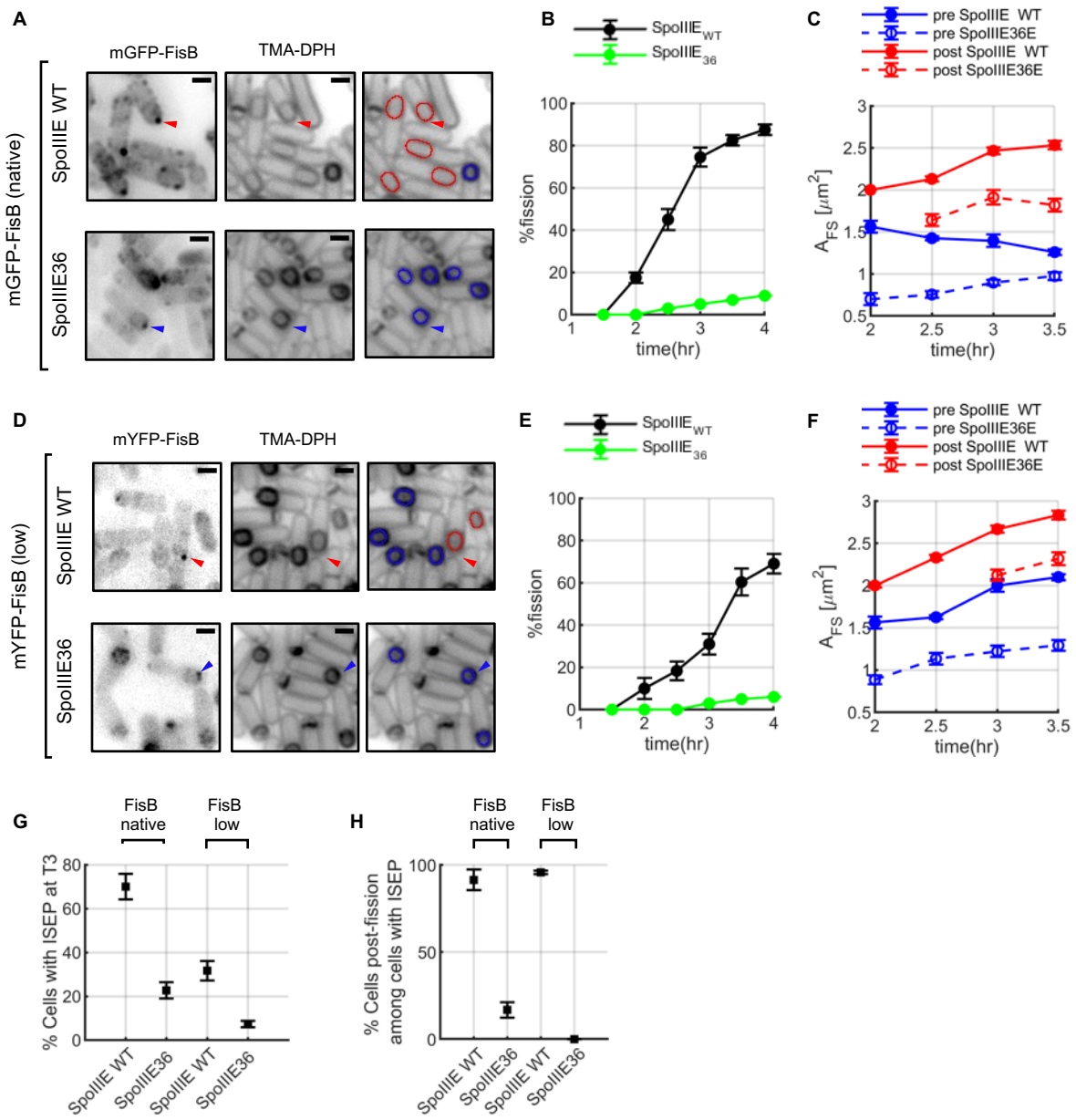

Figure S4. Blocking forespore inflation inhibits membrane fission. Related to Figure 4. A. Engulfment and FisB localization in cells expressing wild-type (WT) SpoIIIE or ATP-ase deficient SpoIIIE36. Membranes were labeled with TMA-DPH and FisB was visualized using mGFP-FisB expressed at native levels on a *ΔfisB* background[S3]. Fluorescence microscopy images were acquired 3 h after nutrient downshift that initiated sporulation. Cells that have visually completed engulfment and had accumulated FisB at the membrane fission site are indicated by arrowheads. On the images on the right, detected FS contours are overlaid in blue and red for pre- and post-fission cells. **B**. Percentage of cells that underwent membrane fission as a function of time into sporulation, for WT and SpoIIIE36 cells. (For each data point >300 cells were analyzed). **C**. FS areas as a function of time after nutrient downshift, for pre- (blue) and post-fission (red) cells, expressing either WT (solid lines) or ATPase deficient SpoIIIE (SpoIIIE36). (n=25-70 cells per data point) **D-F**. As in A-C, but using cells expressing mGFP-FisB at ~8-fold lower levels[S3]. **G**. FisB localization is affected when DNA translocation is

completely blocked. Percentage of cells displaying an intense spot at the engulfment pole (ISEP) for cells expressing SpoIIIE^{WT} or SpoIIIE36 on a background with either native or reduced mGFP-FisB levels. Scale bars = 1 μm. **H.** The fraction of post-fission cells among cells with correct FisB localization (ISEP formation). (n=25-70 cells were analyzed per data point). In panels B,C, E-H, mean±SEM of three independent biological replicates are plotted for every point.

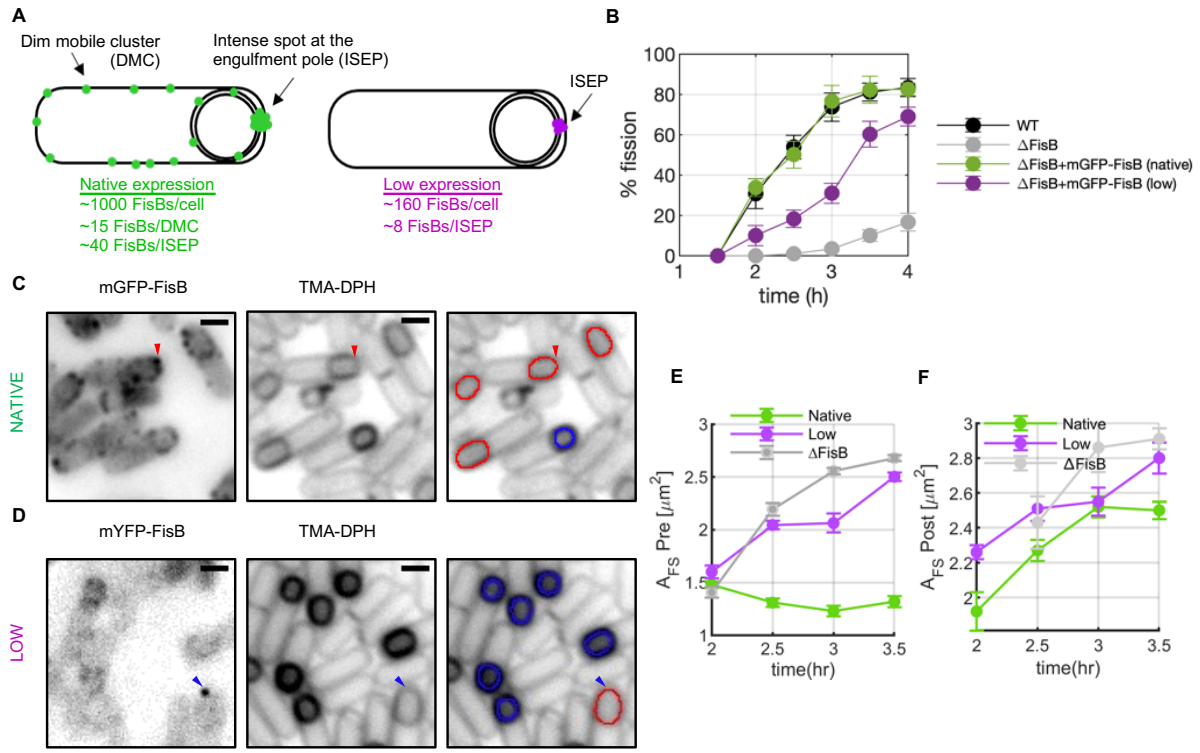

Figure S5. Pre-fission forespores inflate in a low expression FisB strain in which membrane fission is delayed. Related to Figure 5. A. Summary of FisB copy number quantification under native or low expression levels[S3]. Right. Under native expression, on average, there are ~1,000 FisB molecules per cell at t=3 h. Each DMC contains ~12 FisB molecules, while the ISEP contains ~40 FisB copies. In the low-expression strain all the numbers are scaled down ~7-8-fold. **B.** Time course of membrane fission for wild-type cells, *ΔfisB* cells, or *ΔfisB* cells complemented with mGFP-FisB expressed at native (BAM003) or low levels (BAL003). (More than 300 cells were analyzed per data point.) **C.** Fluorescence microscopy images of cells expressing mGFP-FisB at the native level (BAM003) at 3 h into sporulation. Membranes were visualized with TMA-DPH. Examples of a sporulating cell with a discrete mGFP-FisB focus at the cell pole (intense spot at engulfment pole, ISEP) are highlighted with a red arrowhead. In the panels on the right red contours indicate forespores that have undergone fission whereas blue contours indicate forespores that have not yet undergone membrane fission (70 cells per data point). Scale bars represent is 1 μm. **D.** Similar to C but using a strain (BAL003) that expresses mGFP-FisB at lower levels in a *ΔfisB* background. **E, F.** Under mGFP-FisB expression at low levels, both the average pre- (E) and post-fission (F) forespore areas (A_{FS}) grow, in a manner qualitatively similar to cells lacking FisB altogether (ΔFisB). By contrast, for cells expressing mGFP-FisB the native level, the average pre- and post-fission FS areas decrease and increase as a function of time into sporulation, respectively (70 cells were analyzed per data point). Data for *ΔfisB* cells is copied from Figure 6 for comparison. In panels B, E, F, mean±SEM of three independent replicates are plotted.

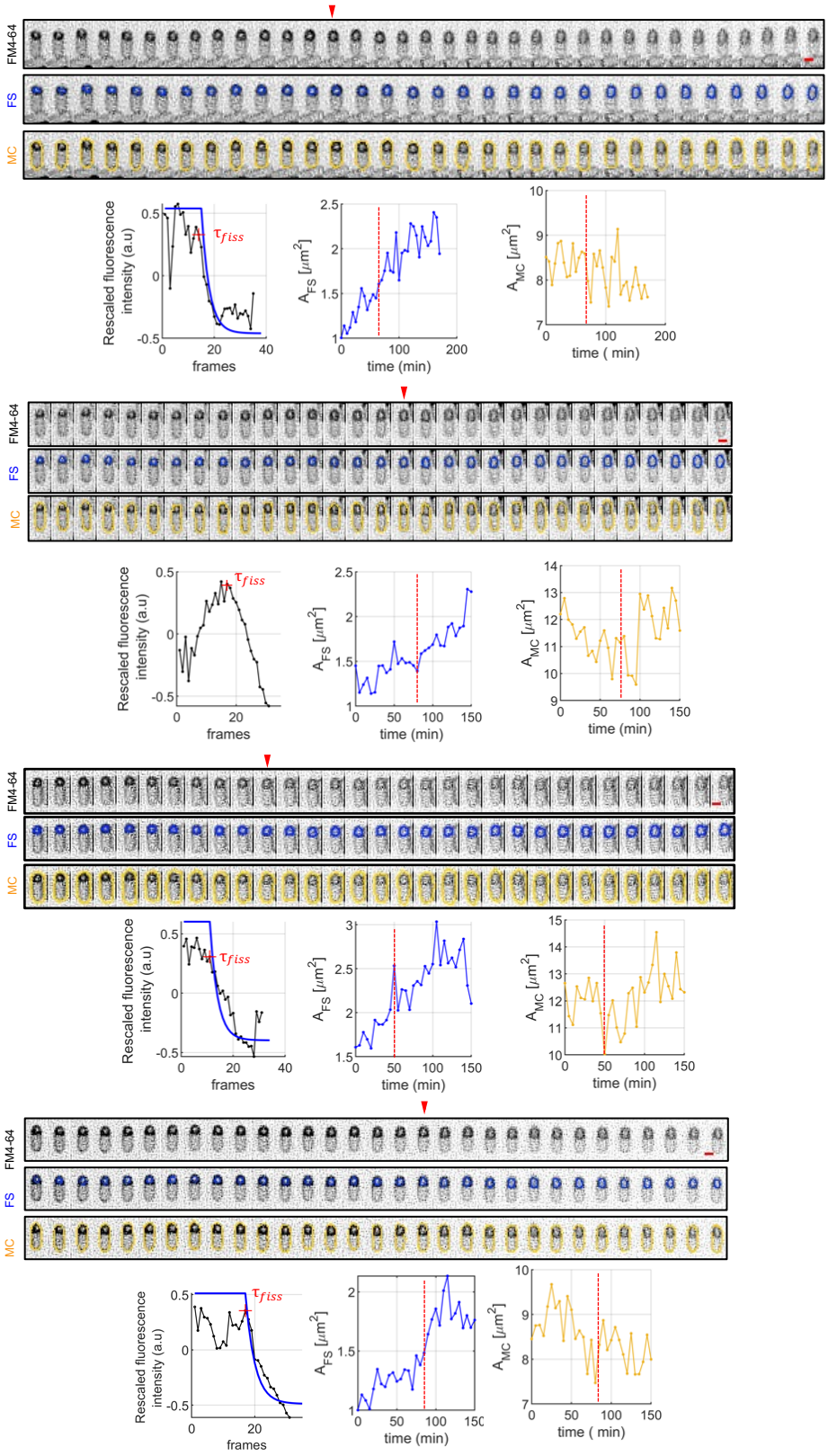

Figure S6. Examples of forespore area growth and membrane fission detected at the single cell level. Related to Figure 6. Each top row of a triplet shows a unique cell followed as

a function of time in time-lapse fluorescence microscopy. Cell membranes were labeled with FM4-64. Images are shown with an inverted look-up table. Frames were acquired every 5 min. The middle and bottom rows of every triplet show the overlaid contour of the FS or the MC membrane, respectively. The intensity of the FS membrane starts decreasing upon membrane fission, because bleached FM4-64 molecules are confined and can no longer exchange with the unlabeled dyes in the bath after membrane fission. For each cell, the mean FS contour intensity and the FS area are shown on the right. The time of membrane fission (τ_{fiss}) estimated from the contour intensity time profile is indicated on the FS area plots.

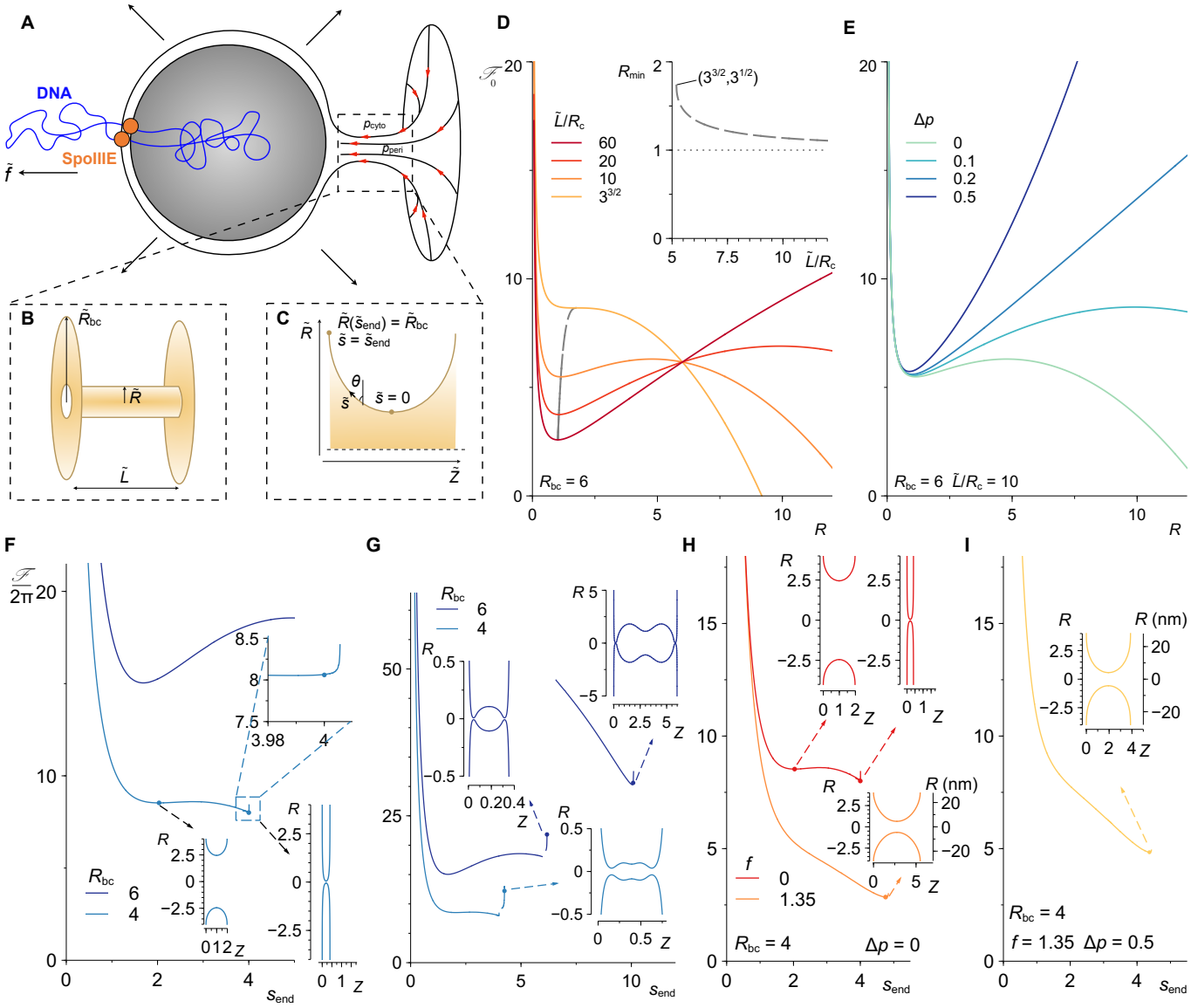

Figure S7. **Free-energy based modeling of the membrane neck. Related to Figure 5**. **A**. Sketch of the engulfment membrane geometry during the last stage of forespore engulfment, showing the flow of lipids through the membrane neck, the osmotic pressure difference $\Delta\tilde{p} = p_{cyto} - p_{peri}$ between the cytoplasm and the periplasm, and the pulling force $\tilde{f}$ due to the SpoIIIE motors translocating DNA into the forespore. **B**. Simplified model of the membrane neck, consisting of a straight cylinder of radius $\tilde{R}$ and length $\tilde{L}$, connecting two planar membranes of radius $\tilde{R}_{bc}$. **C**. Schematic of the more realistic model of the membrane neck showing the parametrization of the surface, where s is the arc length along the contour and θ the angle with respect to the vertical. **D**. Dimensionless free energy $\mathscr{F}_0 = \tilde{\mathscr{F}}_0/(\gamma R_c \tilde{L})$ from Eq. 4 (panel **B**) as a function of the dimensionless neck radius R, highlighting the existence of a local free-energy minimum provided $\tilde{L}/R_c > 3^{3/2}$ (gray dashed curve). Here $R_{bc} = 6$ and $\Delta p = 0$. The inset shows the corresponding radius R_{min} of the local free-energy minimum as a function of $\tilde{L}/R_c$. **E**. Same as in panel **D** but for different values of the dimensionless osmotic pressure difference Δp, for a fixed length of the neck, $\tilde{L}/R_c = 10$. **F**. Dimensionless free energy $\mathscr{F}$ from Eq. 6 (panel **C**) as a function of the arc length s_{end} for different values of the radial boundary size R_{bc}, $f = 0$, and $\Delta p = 0$. The insets show shapes of the neck for $R_{bc} = 4$ and two different values of s_{end}, corresponding to two local minima. The zoomed-in region depicts the sudden increase of free energy as the neck narrows. **G**. Same as in **F** but displaying some of the multiple branches arising for sufficiently large values of s_{end}. **H**, **I**. Same as in **F**, **G** but for $R_{bc} = 4$ and non-zero values of f and Δp. Panel **H** shows $\mathscr{F}$ for two different values of the dimensionless pulling force f, with $\Delta p = 0$, and panel **I** shows the case $f = 1.35$, $\Delta p = 0.5$. The insets show the shapes of the neck for different values of s_{end} indicated with dots.

Supplemental References

S1. Jumper, J., Evans, R., Pritzel, A., Green, T., Figurnov, M., Ronneberger, O., Tunyasuvunakool, K., Bates, R., Zidek, A., Potapenko, A., et al. (2021). Highly accurate protein structure prediction with AlphaFold. Nature *596*, 583-589. 10.1038/s41586-021-03819-2.

S2. Varadi, M., Anyango, S., Deshpande, M., Nair, S., Natassia, C., Yordanova, G., Yuan, D., Stroe, O., Wood, G., Laydon, A., et al. (2022). AlphaFold Protein Structure Database: massively expanding the structural coverage of protein-sequence space with high-accuracy models. Nucleic Acids Res *50*, D439-D444. 10.1093/nar/gkab1061.

S3. Landajuela, A., Braun, M., Rodrigues, C.D.A., Martinez-Calvo, A., Doan, T., Horenkamp, F., Andronicos, A., Shteyn, V., Williams, N.D., Lin, C.X., et al. (2021). FisB relies on homo-oligomerization and lipid binding to catalyze membrane fission in bacteria. Plos Biol *19*. ARTN e3001314, 10.1371/journal.pbio.3001314.